Chemo-Mechanical Interaction in Solid-Solid Reactions

J. R. Bielenberg and Hendrik J. Viljoen
Dept. of Chemical Engineering, University of Nebraska-Lincoln, Lincoln, NE 68588

Deflagrations of solid reactants have been widely studied in the context of self-propagating high-temperature synthesis. Propagating velocities of the order of sound speed or faster have not been contemplated, due to the belief that the processes determining thermal conduction and diffusion cannot support those rates. Experiments, by Enikolopyan, Gogulya and others, however, disproved those notions. A model for solid-solid reactions, which describe deflagration and detonation, is presented. The activation energy is large and the system requires significant preheating before ignition occurs. Based on experimental observations, the activation energy of a compressed system is lowered by the amount of elastic work done during compression. This phenomenon is included in the model. Ignition by impact and external thermal sources are investigated, and detonations develop only in the case of impact initiation. Interactions between the shock front and the reaction front are also investigated.

Introduction

Fast solid-solid reactions represent an area of reaction kinetics, which is both very important and poorly understood. If the solid-solid reaction is strongly exothermic, we can expect a rich spectrum of new physical phenomena. Since heat generation of solid-solid reaction can easily reach parameter values typical for explosive materials, we can contemplate phenomena of solid-solid detonation. Davis et al. (1998) reported on these type of reactions for Ti + teflon and Fe_2O_3 + Al + teflon. In both cases thermal decomposition of the teflon liberates the very reactive fluorine compound. Their experimental results are corroborated by a Zeldovich-Neumann-Doring (ZND) model and a detonation velocity of ≈ 3.4 km/s has been found.

Earlier evidence of solid-phase detonation goes back to the work of Enikolopyan (1989, 1991). His findings are based on experimental work done with a variety of materials in a Bridgeman anvil. Wafers of solid material were placed in a die and longitudinally or shear loaded. Reactions occur at extremely high rates, with little or no release of the heat of reaction. In one instance hydrated copper sulfate was mechanically activated, and, after a fast decomposition reaction, elemental copper was found in the die. In another experiment the decomposition of ammonium dichromate was investigated. The adiabatic temperature rise for this reaction is 1,300°C, but they only measured temperature rises in the order of 300°C. Eighty percent of the available chemical energy was used to support an elastic shock wave that propagated through the sample at a speed of $\approx 2{,}200$ m/s. The reaction front lagged the shock wave, but it still propagated at a velocity of 1,300 m/s. They provide several other examples as evidence that chemical energy is not necessarily released in the form of heat. Enikolopyan also found that the critical mechanical load to initiate the fast reaction depends on the compact's thickness. As the wafer thickness increases, the critical load decreases to initiate fast reactions, but there exists a minimum wafer thickness below which mechanical activation does not occur. These results underscore our lack of understanding how mechanical and chemical effects interact.

Solid-phase reactions also do not follow Arrhenius rate dependence under all conditions. This experimental observation points to a change in the activation energy of a solid-solid system when it is compressed. The lowering of the activation energy makes the mixture more reactive, and reaction can start at lower preheating. Benderskii et al. (1989) addressed this question of ''activation'' of a solid-phase reactive species by either thermal or mechanical means. To study the latter phenomenon, mechanical activation was studied for reacting

Correspondence concerning this article should be addressed to H. J. Viljoen.

mixtures at temperatures below 60 K. When a mixture is compressed, the elastic potential energy is increased and the global activation energy is decreased.

Knyazeva and Dyukarev (1995) used the reduction of activation energy by mechanical loading to model the problem of steady-state propagation. They found four different propagation velocities, counting the kinetically controlled solution. A second solution is the typical SHS reaction, but the other two are subsonic and supersonic propagating states. Viljoen and Hlavacek (1997) included non-Fourier conduction in their analysis and also found fast deflagration and detonation solutions. Knyazeva (1993) also did a stability analysis of the deflagration and detonation solutions and found oscillatory instabilities when the stability threshold of the bifurcation parameter is exceeded. This result is not surprising, since the problem is quite similar to the traditional SHS problem. Sivashinsky (1981) showed that SHS propagation can be destabilized, and a variety of new modes can develop which are associated with two- and three-dimensional spatial structures. It is therefore highly likely that symmetry breaking can occur in SHS deflagration and detonation.

In another series of experiments, Nesterenko and coworkers used an explosive to collapse copper cylinders filled with Mo + Si powders, Ti + Si, Nb + Si, and so on. The average particle sizes of the powders which were used in these experiments were more than 1 μm. Nesterenko et al. (1994, 1995) studied the structure of the reactive porous powders after compression by an explosive. Particle melting, changes in morphology, and partial reaction have been observed. High shear rates are encountered during the explosion, causing the more malleable powders to deform into thin parallel layers. This results in an increase in the contact area between reactants. Inside the shear bands vortices formed. A numerical study of this process was done by Benson et al. (1995). The focus of their work was on the effects of high strain rates on the mechanical, physical, and to a lesser extent chemical properties of a mixture of reactive powders. Chen et al. (1998) subjected Ti − Si mixtures to varying strains. It was not the collapse of pores that initiated reactions. Instead strains above a threshold value ≈ 10 initiates reaction inside the shear bands, and propagation occurs through the specimen at strain values ≈ 20–40. Vreeland et al. (1997) investigated shock-induced reactions for the Ti − Si system. Threshold shock energy for complete conversion was found, and it was correlated with the melting temperature of Si. The threshold increased for larger initial particle sizes and lower porosities. This result is expected. For larger particles, poorer mixing can be expected in shear bands. It is also known that shock temperatures increase with initial porosity.

An excellent review of shock-induced chemical reactions was made by Thadhani (1993). The phenomenological processes which occur prior to shock-induced reaction are (1) formation of defects; (2) plastic deformation, void collapse, and heating due to viscoplastic flow; (3) turbulent-like flow with intense mixing; (4) fissure and cracking to expose surfaces with dangling bonds. Thadhani also notes that energy released in shock-induced reactions is primarily in the form of heat, however, the melting temperatures of reactants or products are not always exceeded and condensed phase reactions are commonly found, for example *W* and *Re* reaction (Thadhani et al., 1991). The exact mechanism (or mechanisms) of the reaction is still not clear, and several kinetic models have been proposed, for example, Maiden et al. (cf. Thadhani, 1993, p. 192) and Horie and Kipp (1998). Temperature dependence is of the Arrhenius type and the order of the reaction is usually first-order if mixtures are assumed to be homogeneous. Horie and Kipp (1988) considered a two-step mechanism with the formation of an intermediate product, followed by a transformation to the final product. Only the first step involves two-body interaction, which involves the issue of mixing. The frequency factor for this step is varied linearly with the strain rate to account for the influence of hydrodynamical motion on mass mixing, but the basis for this is empirical. Bennett et al. (1994) used this kinetic model in a heterogeneous system, finding reasonably good agreement with experimental systems Ni − Al and Al − Fe_2O_3. A more detailed description of the particle-particle interaction is given by Yano and Horie (1998). This description is based on discrete element modeling (DEM), an approach that accounts for the tracking of individual particles, similar to a molecular dynamics model. DEM reveals that particle velocity distributions could reach kinetic energy levels that could cause submicron-level mixing, thus providing the driving mechanism for ultrafast chemical reactions in the shock front. The validity of an Arrhenius type model is questionable. Benderskii et al. (1989) and experimental results by Enikolopyan (1991) indicate that activation energy is lowered by elastic compression of reactants. This phenomenon is included in this article.

Another issue that is unresolved is the mechanism of the mass-transfer rate. The findings by Nesterenko and coworkers that reactions first initiate in the shear bands is not merely an indication of higher temperatures in those zones, but also improved mixing. Batsanov (1996) proposed that mixing is accomplished by differences in the particle velocities of constituents. Faster traveling particles of one species penetrate other particles to create intimate mixing. Graham (1997) has developed a model to explain the mechanisms of shock-induced solid-state reactions. He identifies four sequential processes, configuration (initial porosity, powder morphology), mixing, activation, and heating (cf. Graham, 1997, and references therein). He concludes that many of the material descriptions are unknown and many models can be fit to isolated sets of data, but a comprehensive description is still lacking.

Juxtaposed to shock-induced reactions are conventional SHS reactions. These reactions propagate as deflagrations through a premixed compact at velocities of a few mm to a few cm per second. The mechanical coupling with stress is primarily through thermal stresses and quasi-static descriptions of the thermoelastic (or thermoviscoplastic, depending on constitutive description) suffice. The common view is held that no feedback occurs that affects the kinetics; thus, displacement vectors (and stresses) can be solved separately. New experimental results are changing this view. Varma et al. (1998) have used microscopic high-speed video recording to study reaction fronts *in situ* in the Nb + B system, where the adiabatic temperature is below the melting temperatures of both reactants. Periodic cracking has been observed just ahead of the reaction front, and this induces oscillations in the propagation velocity. This is clearly an example where mechano-chemical interactions are present in low-speed de-

flagrations. A transition occurs as the deflagration velocity increases, approaching cold sonic values. Higher deflagration velocities are reached for mixtures of ultrafine powders which are mixed on the ''micro-to-nano'' level, diffusion resistance of solid-solid reactions is suppressed and the propagation velocities of the SHS deflagration is in the range 10–800 m/s (Danen and Martin, 1993; Aumann et al.., 1995). Eventually, for a detonation SHS regime, the propagation velocities can be in the range of 4–10 km/s (Gogulya, 1992; Kovalenko and Ivanov, 1981). Strong coupling now exists between chemical and mechanical processes.

There is a growing body of experimental evidence that solid-solid combustion waves can couple with shock waves to produce very high propagation velocities. There exists a synergism between shock compression and chemical activation. Reactions can strengthen shock waves, and compression can activate reactive mixtures. A systematic analysis of this problem is necessary to explain the experimental observations and direct experimentalists to system which are likely to exhibit these phenomena. In this article we present an analysis of the solid-phase mechano-chemical problem for the case of perfectly mixed reactants. The activation depends on both temperature and elastic compression, as suggested by Benderskii et al. (1989). The mathematical model is valid for conditions well above the Hugoniot elastic limit (HEL), where the state variable pressure applies and the solid's compressibility becomes significant. An equation of state for the solid is based on the Mie-Grüneisen equation that equates total pressure with the sum of a cold compression part and a thermal pressure. The effects of impact velocity and preheating are investigated, and the interaction between the shock wave and the reaction wave are demonstrated in the examples.

Mathematical Model

Consider a mixture of reactive powders pressed into the shape of a cylinder. In this analysis it is assumed that the powder has been compressed to the standard density of the system, that is, no pores are present. Furthermore, we do not distinguish between immiscible phases, since that would require additional equations of state, energy, and momentum balances for each phase, and the description of exchange of energy and momentum between phases will complicate the model to the point where it could obfuscate the features which can be captured with the current model.

The cylinder is placed in an ampoule, and it is assumed that the walls of the ampoule are rigid and perfectly insulated (adiabatic system). A one-dimensional description of the system, coinciding with the axial variable of the cylinder is used. The mixture is strongly exothermic and the activation energy is high, typically in the order of 10^5 J/mol. Although we deal with a solid material, it is important to realize that the material behaves like a fluid when it is shocked well beyond the Hugoniot elastic limit and particle velocities can reach large values. An important consequence of this particle flux is that thermal and mass convection can augment the slow transport processes of thermal conduction and diffusion. Also, the coupling of compression in the thermal component of internal energy plays a key role in initiating the detonation reaction. The stress tensor consists primarily of the three (equal) principal components in the plastic state and is substituted with the state variable pressure. The system is compressible, a necessary requirement when pressures of several hundreds of thousands of atmospheres are considered.

The continuity equation is

$$\frac{\partial \rho}{\partial t} + \frac{\partial \rho u}{\partial x} = 0 \tag{1}$$

where ρ and u denote density (kg/m^3) and particle velocity (m/s) of the material. The momentum balance can be written in Euler form

$$\frac{\partial \rho u}{\partial t} + \frac{\partial \rho u^2}{\partial x} = -\frac{\partial P}{\partial x}. \tag{2}$$

The concentration balance is expressed in terms of a mass fraction X_f

$$\frac{\partial \rho X_f}{\partial t} + \frac{\partial \rho u X_f}{\partial x} = -k_o \rho X_f e^{-E/RT}. \tag{3}$$

The internal energy balance (J/kg) consists of thermal ($\epsilon_T = C_v(T - T_o)$) and kinetic components

$$\frac{\partial \rho \epsilon_T + \rho u^2/2}{\partial t} + \frac{\partial \rho u\left[\epsilon_T + u^2/2\right]}{\partial x} = -\frac{\partial Pu}{\partial x} + (-\Delta H) k_o \rho X_f e^{-E/RT} + \frac{\partial}{\partial x} k \frac{\partial T}{\partial x}. \tag{4}$$

The system is closed by an equation of state. There are marked differences in high-pressure effects of gases and solids. The pressure in a gas is of thermal origin and is directly proportional to temperature. The compressibility of a gas is much bigger than for a solid, and the limiting compression $(\gamma + 1)/(\gamma - 1)$ (γ is the polytropic coefficient) is achieved across a shock wave of tens or a few hundred atmospheres. The behavior of a condensed phase to compression is altogether different. Under ambient conditions, atoms maintain an average distance from each other to equilibrate attractive binding and repulsive nuclear forces. For comparison with the gaseous state, to compress a cold metal to 90% of its original volume requires external pressure of 10^5 atm. To reduce the volume by 50% requires a pressure of several million atmosphere (cf. Trunin, 1998). The pressure P consists of two contributions: (a) cold compression (no thermal effect) of solids leads to huge internal pressures caused by repulsive nuclear forces; (b) the material is strongly heated by a shock wave leading to additional pressure rise of a thermal origin. The thermal component of the pressure consists of nuclei vibration and electron thermal pressure. The contribution from the electrons to the overall pressure only becomes significant above tens of thousand degrees Kelvin. Neglecting electron thermal pressure, the total pressure (Pa) is

$$P = P_c + P_T. \tag{5}$$

The relation between P_c and ρ is often referred to as the constitutive relation. Shchetinin (1991) proposed the follow-

ing constitutive equation. Let K_{T_o} denote the bulk modulus of isothermal compression (Pa) at the initial temperature and $\chi = 1 + (\partial K_{T_o}/\partial P)|_{T_o, P_o}$, then P_c is given by

$$P_c = \frac{K_{T_o}}{\chi}\left(e^{\chi(1-\rho_o/\rho)} - 1\right) \tag{6}$$

Remark: This equation can be compared to alternatives like the Murghanan equation or the Born-Mayer interaction potential.

The Mie-Grüneisen equation (cf. Ahrens, 1993) describes the relation between thermal pressure and the thermal component of the internal energy ϵ_T as follows

$$P_T = \frac{\Gamma}{\upsilon}\epsilon_T = \frac{\Gamma C_\upsilon}{\upsilon}(T - T_o) \tag{7}$$

where Γ is the Grüneisen coefficient. Combining Eqs. 6 and 7, the two-term equation of state is obtained

$$P = \frac{K_{T_o}}{\chi}\left(e^{\chi(1-\rho_o/\rho)} - 1\right) + K_{T_o}\alpha_T(T - T_o) \tag{8}$$

where the thermal expansion coefficient α_T (K^{-1}) is related to the Grüneisen coefficient $\alpha_T = \Gamma(\upsilon_o)C_\upsilon/\upsilon_o K_{T_o}$. In this analysis we make use of the assumption that the ratio of the Grüneisen coefficient to specific volume remains constant, that is, $\Gamma/\upsilon = \Gamma(\upsilon_o)/\upsilon_o$ (cf. Dijken and De Hossen, 1994) for this and other functional relations for Γ. By using this EOS, we tacitly assume that the system remains in a condensed state. A similar EOS could be used for a liquid phase. Therefore, the reference to solid-solid reaction in this text refers to the initial state of all reactants and it also implies the use of the two-term EOS (Eq. 8).

Another important assumption is perfect mixing. It is assumed (by the form of the reaction) that the limiting reactant is perfectly mixed with the other reactants. In this model we do not account for different phases. A model that takes the heterogeneous nature of constituents into account requires separate momentum and internal energy balances and equations of state for the different species (cf. Akhmadeev, 1997; Baer, 1997). Also, provision must be made for exchange of momentum and internal energy between phases across phase interfaces. These relaxations do not necessarily occur on time scales comparable to the residence time within the shock wave, and a nonequilibrium state can persist in the post-shock region. To bring this aspect in perspective with the work presented in this article, perfect mixing is assumed and the rate of reaction depends on the availability of a single compound and temperature.

When conduction and viscosity are neglected, Eqs. 1, 2, and 4 can be integrated over an infinitesimally thin sheet where the shock is located to give, after minor manipulation, the Rankine-Hugoniot equations (usually in the absence of reaction). The Rankine-Hugoniot equations can be used to construct Hugoniot curves (Zeldovich and Raizer, 1967). The Hugoniot constitutes a locus of end states (typically P vs. $1/\rho = \upsilon$) and different positions on the curve cannot be reached from the same initial conditions.

In order to include reduction of activation energy by elastic compression in our analysis, we turn to Benderskii et al. (1989) who proposed the following

$$E = E_o - \alpha\epsilon_c. \tag{9}$$

Since $\epsilon_c = -\int_{\upsilon_o}^{\upsilon} P_c\, d\upsilon$, Shchetinin's equation can be used to express ϵ_c in terms of specific volume. The activation energy is a function of υ, and it is described by the dimensionless function $Z(\upsilon)$ as follows

$$E(\upsilon) = E_o Z(\upsilon) \tag{10}$$

and $Z(\upsilon)$ is

$$Z(\upsilon) = 1 - \frac{\alpha M_M K_{T_o}\upsilon_0}{E_0\chi^2}\left[e^{\chi[1-(\upsilon/\upsilon_o)]} - 1 + \chi\left(\frac{\upsilon}{\upsilon_0} - 1\right)\right]. \tag{11}$$

M_M is the molar mass in kg/mol and α is a dimensionless parameter ($0 \le \alpha \le 1$) termed the sensitivity parameter (cf. Shlensky, 1995, for an interesting discussion on sensitivity). Reactants which are ignited by slight impact are considered sensitive and $\alpha \approx 1$. In this study both $\alpha = 1$ and $\alpha = 0$ will be investigated.

The following scales are introduced to render the equations dimensionless. The cold sonic velocity, $a_o = \sqrt{K_{oT}/\rho_o}$ is used as a scale for velocity, that is, u/a_o. Pressure is scaled as $(P - P_o)/\rho_o a_o^2$. Let L_s denote a length scale, still to be defined, then time can be scaled by L_s/a_o. The density is scaled with the fully dense solid state under ambient conditions ρ_o. The dimensionless temperature is defined as $(T - T_o)/(T_a - T_o)$, where T_a denotes the adiabatic temperature (K) at atmospheric pressure. The length scale L_s is chosen as 20×10^{-6} m. Although this length scale is not a natural choice for the system, this length accounts for at least ten particle diameters (the continuum model breaks down at the particle diameter length scale), and it is also used as the step size in the spatial discretization. Therefore, $\Delta x = 1$ after scaling.

The same symbols can be used without confusion for the scaled variables. In dimensionless form, the governing equations can be written as

$$\frac{\partial\rho}{\partial t} + \frac{\partial\rho u}{\partial x} = 0 \tag{12}$$

$$\frac{\partial\rho u}{\partial t} + \frac{\partial\rho u^2}{\partial x} = -\frac{\partial P}{\partial x} \tag{13}$$

$$\frac{\partial}{\partial t}\left[\beta_1\rho T + \rho u^2/2\right] + \frac{\partial}{\partial x}\left[\beta_1\rho u T + \rho u^3/2\right] = -\frac{\partial Pu}{\partial x} + \beta_2 Da\rho X_f e^{\gamma\left(\frac{T+\delta-(\sigma+1)Z}{T+\sigma}\right)} + \beta_3\frac{\partial^2 T}{\partial x^2} \tag{14}$$

$$\frac{\partial}{\partial t}\left[\rho X_f\right] + \frac{\partial}{\partial x}\left[\rho u X_f\right] = -Da\rho X_f e^{\gamma\left(\frac{T+\delta-(\sigma+1)Z}{T+\alpha}\right)} \tag{15}$$

$$P = \frac{1}{\chi}\left[e^{\chi(1-1/\rho)} - 1\right] + \beta_4 T. \tag{16}$$

Neuman boundary conditions are used except where it is

stated otherwise in the examples which follow. The dimensionless parameters are defined in the Notation.

Numerical Solution of Model

Numerical modeling of reactive compressible flows are notoriously difficult. Most studies deal with reactive gaseous systems, and the ideal gas law remains a popular equation of state. In this case the equation of state is quite different and the parameters of the system correspond to the solid state. The solution is limited to a single spatial variable, coinciding with the axial variable of the cylinder. A finite difference method is used to solve this problem. The flux corrected transport (FCT) method of Boris and Book (1976) has proved to be an effective method to resolve the steep gradients, which are present in the shock zone. The method can be briefly described at the hand of the following generic problem

$$\frac{\partial A}{\partial t} + \frac{\partial uA}{\partial x} = 0.$$

Let $[A_i^t]$ denote the discretized set at time t (s) and let δt be the time step. FCT is essentially a two-step process. First, $\bar{u}_{i+1/2} = 0.5(u_i^t + u_{i+1}^t)$ is calculated, as well as the parameters

$$\epsilon_{i+1/2} = \bar{u}_{i+1/2}\,\delta t$$

and

$$\nu_{i+1/2} = 0.5\left[0.5|\epsilon_{i+1/2}| + 0.25\left(1+\epsilon_{i+1/2}^2\right)\right]. \qquad (17)$$

Remarks: ϵ must satisfy $|\epsilon| < 1$ (which determines an upper bound on δt) and ν must satisfy: $0.25(1+\epsilon_{i+1/2}^2) \geq \nu \geq 0.5|\epsilon_{i+1/2}|$ to guarantee positivity and stability. Equation 17 reflects a choice of ν midway between the two bounds.

The first step is diffusive and the intermediate values $[\bar{A}_i]$ are calculated as follows

$$\left[\bar{A}_i\right] = aA_{i-1}^t + bA_i^t + cA_{i+1}^t$$

where

$$a = \nu_{i-1/2} + 0.5\epsilon_{i-1/2},$$

$$b = 1 - 0.5\epsilon_{i+1/2} + 0.5\epsilon_{i-1/2} - \nu_{i+1/2} - \nu_{i-1/2}$$

and

$$c = \nu_{i+1/2} - 0.5\epsilon_{i+1/2}.$$

Next, antidiffusion fluxes are calculated to correct the strong diffusion introduced in the first step. The antidiffusion coefficients are: $\bar{a}_{i+1/2} = \nu_{i+1/2} - 0.5\epsilon_{i+1/2}^2$ and the raw antidiffusive fluxes (uncorrected values) are $R_{i+1/2} = \bar{a}_{i+1/2}(\bar{A}_{i+1} - \bar{A}_i)$. Let S denote the sign of $(\bar{A}_{i+1} - \bar{A}_i)$ and $B = \min[S(\bar{A}_{i+2} - \bar{A}_{i+1}),\ |R_{i+1/2}|,\ S(\bar{A}_i - \bar{A}_{i-1})]$. The corrected fluxes are $C_{i+1/2} = S\max[0, B]$, and, in the second step, the diffusive step is corrected

$$A_i^{t+\delta t} = \bar{A}_i - C_{i+1/2} + C_{i-1/2}.$$

Table 1. Parameter Values

Property	Value	Units
E_o	$(0.5 \text{ or } 1.0)\times 10^5$	J/mol
K_{oT}	69.1×10^9	Pa
L_s	20×10^{-6}	m
ρ_o	4,000	kg/m^3
C_v	1,000	J/(kg·K)
$(-\Delta H)$	4×10^6	J/kg
k	40.0	W/(m·K)
T_o	300	K
X_{fo}	0.5	
α_T	5.0×10^{-5}	K^{-1}
χ	6.1	

There are some adjustable parameters in this method (see Boris and Book, 1976, for details), for example, the inequality mentioned in the Remarks section allows some variation in the calculation of ν. In the antidiffusive step no existing maximum or minimum value is accentuated and this is evident from the way B is determined.

Results

Example I

First, consider a system that is only preheated at the one end. The activation energy of the system was set at 100 kJ/mol and the heat of reaction was 4,000 kJ/kg. Other relevant parameter values are given in Table 1. The sample is preheated at one end ($x = L$) to 50% of the adiabatic temperature value

$$T(0, L) = 0.5 \qquad (18)$$

The other initial conditions are

$$P = \rho - 1 = X_f - 0.5 = u = 0. \qquad (19)$$

This initial state constitutes a system at rest, where an instantaneous temperature profile is established at $t = 0^+$. In practical terms, this state can be approached with intense laser heating. A thermal shock wave propagates through the medium to relieve the thermal stress. This is illustrated in Figures 1 and 2 where pressure and temperature profiles are shown at 3 instances in time. The shock wave propagates in

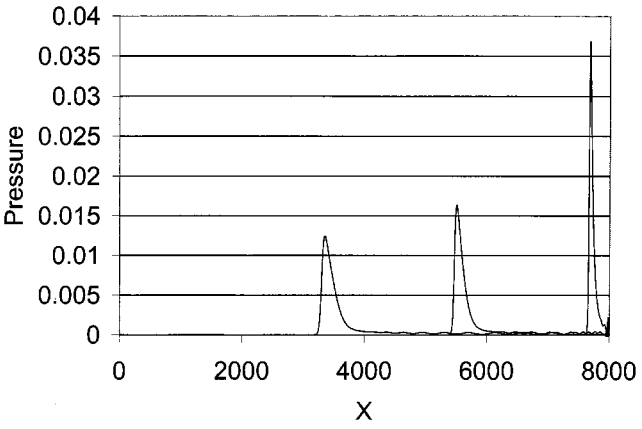

Figure 1. Pressure profiles at t = 4,500 and 6,500.

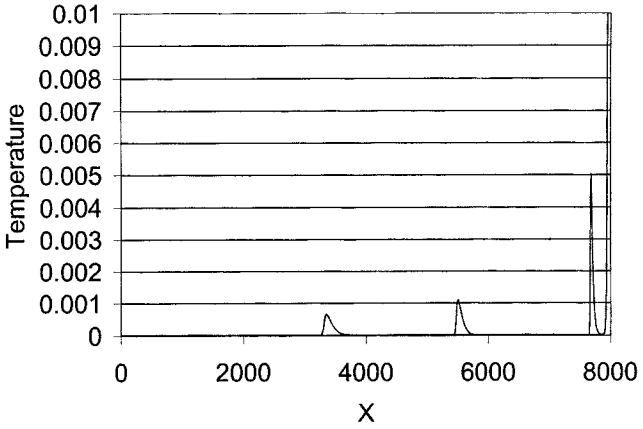

Figure 2. Temperature profiles at $t = 4{,}500$ and 6,500.

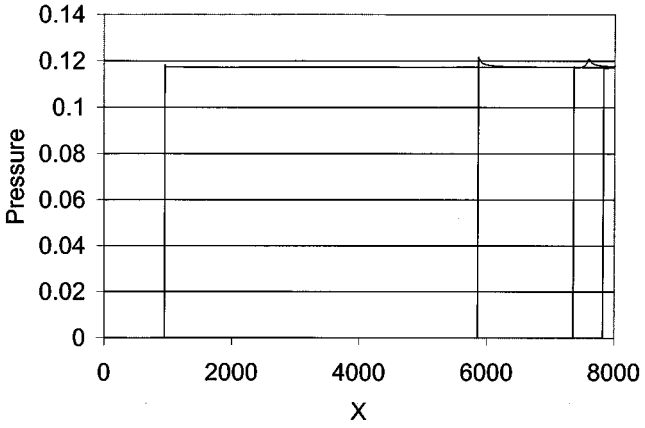

Figure 3. Pressure profiles at $t = 200$; 600; 2,000; and 6,600.

the form of a pulse from right to left in the figures. The pressure pulse is small and the compression that occurs in the pressure wave gives rise to a slight temperature rise. When the material relaxes, the temperature decreases and the temperature pulse travels with the pressure pulse at a velocity of Mach 1, as one would expect from an acoustic wave. Strictly speaking, a thermoelastic description should have been used, since the material was not strained beyond the Hugoniot elastic limit. However, the results will look qualitatively the same in both cases (cf. Viljoen and Cohn, 1998).

Ignition occurs at $x = L$, due to the preheating, and a large rise in temperature is noted. The position of this temperature rise does not appear to move over the integration period of $t = 4{,}500$. This period translates into a real time of $400\,L_s/a_o = 21.6$ μs. Combustion velocities of typical SHS systems are in the order of 1 cm/s. That would correspond to a dimensionless velocity of 2.4×10^{-6}. Over the time frame shown in these profiles, that velocity would cause a displacement of only 0.01 position units. Even SHS deflagrations with propagation velocities of 10 m/s will exhibit only a slight change on this time scale.

When the calculation is repeated for $\alpha = 1$, the resulting temperature, pressure, and conversion profiles are identical. This is expected, since the magnitude of the pressure is very small and insignificant reduction of activation energy will occur.

Example II

In this example, the system is both preheated and shock-compressed. The activation energy E_o is 50 kJ/mol. The other parameter values are listed in Table 1. The initial pressure, density, and mass fraction profiles remain the same as in the previous case, but the temperature and velocity profiles are given by

$$T(0, x) = 0.2\,e^{(x-L)/10}$$

$$u(0, x) = 0.1.$$

The sample is now traveling towards a stationary wall with velocity $u = 0.1$, and at $t = 0^+$, it impacts the wall ($a_o = 4{,}167$ m/s and, hence, the impact velocity is only 417 m/s). The boundary condition at the impact point is $u(0, L) = 0$ and a shock wave travels from $x = L$ into the system.

In the first case $\alpha = 0$. The pressure and temperature profiles are shown in Figures 3–4 at $t = (200; 600; 2{,}000; 6{,}600)$. A slight peak is noticeable in the pressure profile at $t = 600$, but a steady wave is established with constant propagating velocity $D = 1.08$. The slight rise in pressure at the edge of the wave at $t = 2{,}000$ is not due to Gibb's phenomenon. Note that it has a distinct spatial form, and it is a result of the small pressure peak (that was present at $t = 600$ behind the front), which has overrun the wave. The pressure rise is only 0.118, and the compression is not sufficient to ignite the system. A thermal wave travels along with the shock wave, but the temperature rise associated with it is small, $T = 0.05$. Ignition has occurred at $x = L$, due to preheating and the position of the deflagration is clearly noticeable in Figure 4 at $t = 6{,}600$ near $x = L$.

Repeating the calculation for $\alpha = 1$ clearly illustrates the effect of activation energy reduction by shock compression. The pressure profiles are shown in Figures 5a–5b at $t = (3{,}800; 4{,}400; 4{,}600; 4{,}800; 5{,}600; 6{,}800)$. At $t = 3{,}800$ and 4,400, the pressure wave shows no irregular behavior and the propagation velocity is $D = 1.08$. Careful investigation of the

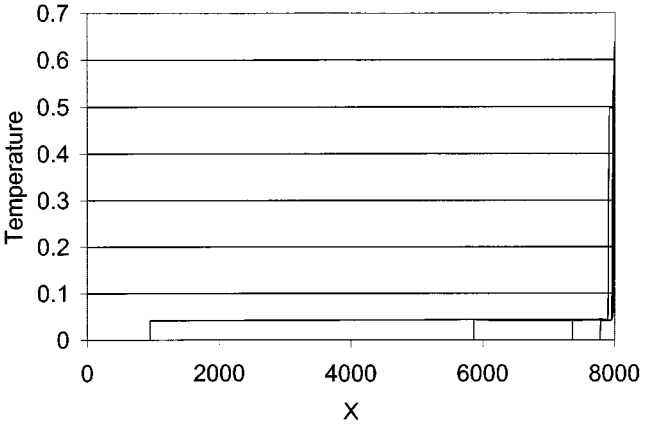

Figure 4. Temperature profiles at $t = 200$; 600; 2,000; and 6,600.

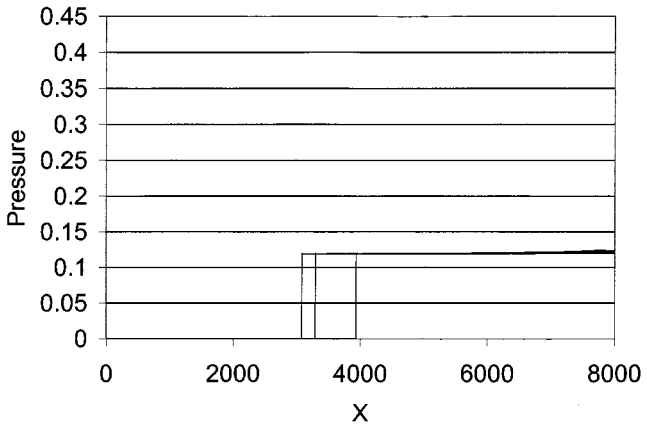

Figure 5a. Pressure profiles at $t = 3{,}800$; 4,400; and 4,600.

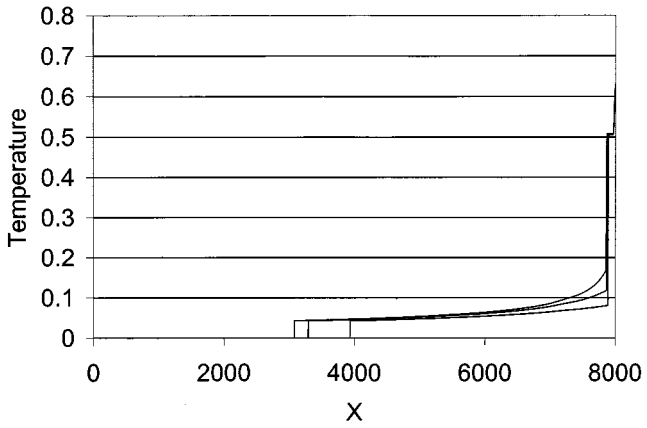

Figure 6a. Temperature profiles at $t = 3{,}800$; 4,400; and 4,600.

profile at $t = 4{,}600$ shows a slight rise in pressure near $x = L$, and, at $t = 4{,}800$, a clear pressure pulse has formed near $x = L$. This pulse travels downstream with a velocity of $D = 1.58$ (6,583 m/s). The position of the pressure spike corresponds to the location of the vertical section of the reaction front (cf. Figure 7b). As time progresses, the pressure spike grows larger with pressure values ranging from 0.193 (133,000 atm) at $t = 4{,}800$ to 0.421 (290,000 atm) at $t = 12{,}000$. The spike moves along with the reaction front at 1.58 times the cold sonic velocity. The spike also appears to widen as time progresses. The leading edge of the spike is nearly vertical and corresponds exactly with the vertical part of the reaction front.

The temperature profiles are shown in Figures 6a–6b. The shock compression causes a sufficient reduction in activation energy to initiate chemical reaction directly behind the shock front. This can also be discerned from the gradual rise in the temperature profile behind the shock wave (see Figure 6a, $t = 3{,}800$). Ignition has occurred at $x = L$ and the movement of the deflagration, identified by the sharp increase in temperature, can be followed by comparing Figures 6a–6b. At $t = 4{,}800$, a slight increase in temperature develops at the deflagration front. A transition from a deflagration to a detonation occurs, and, at $t = 5{,}200$, the detonation is positioned at $x = 7{,}500$ traveling at a velocity of $D = 1.58$. The detonation is associated with the sharp pressure pulses shown in Figure 5b. The temperature behind the reaction front does not reach the (atmospheric pressure) adiabatic value of the reaction $T = 1$. A temperature spike occurs at the step between the two temperature plateaus in Figure 6b. Its position corresponds to that of the pressure pulse and reaction front. Its value ranges from .55 at $t = 5{,}000$ to .74 at $t = 6{,}800$.

The mass fraction X_f is depicted at $t = (3{,}800; 4{,}400; 4{,}600; 4{,}800; 5{,}200; 6{,}800)$ in Figures 7a–7b. Partial conversion occurs between the leading shock front and the deflagration, as can be noted from Figure 7a. After 4,000 time units, the reaction starts to progress at a much more rapid rate. The reaction front takes on a new shape. Between 4,800 and 5,000 time units, the main reaction zone still appears to be deflagrating slowly, but increased conversions of as much as 25–30% occur between the position of the compression wave and the reaction front. At approximately 5,600 time units, the reaction zone begins to propagate at a rate that is much faster than its former velocity. A nearly vertical reaction front is formed which moves toward the shock wave at the velocity of $D = 1.58$. The front becomes steeper. This implies that the reaction zone is thinning. At $t = 6{,}800$, the mass fraction of

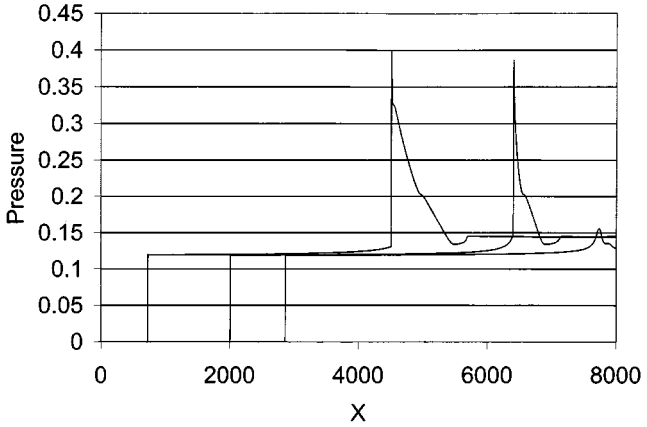

Figure 5b. Pressure profiles at $t = 4{,}800$; 5,600; and 6,800.

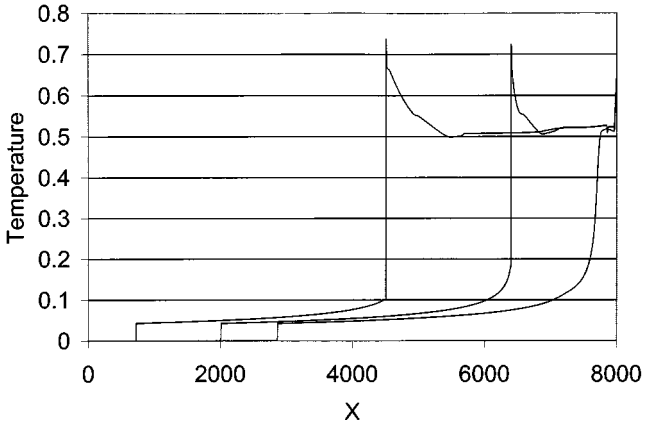

Figure 6b. Temperature profiles at $t = 4{,}800$; 5,600; and 6,800.

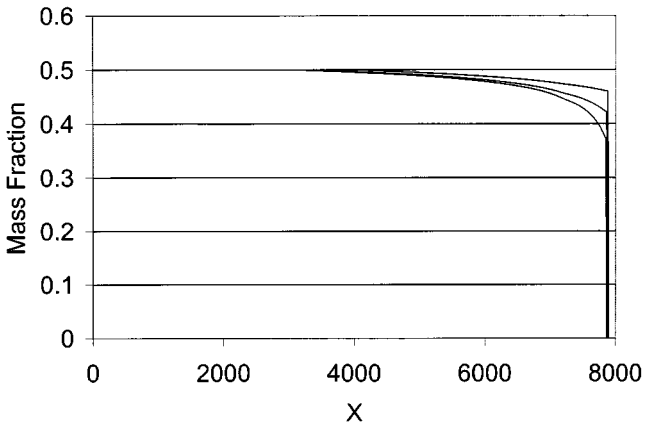

Figure 7a. Mass fraction profiles at t = 3,800; 4,400; and 4,600.

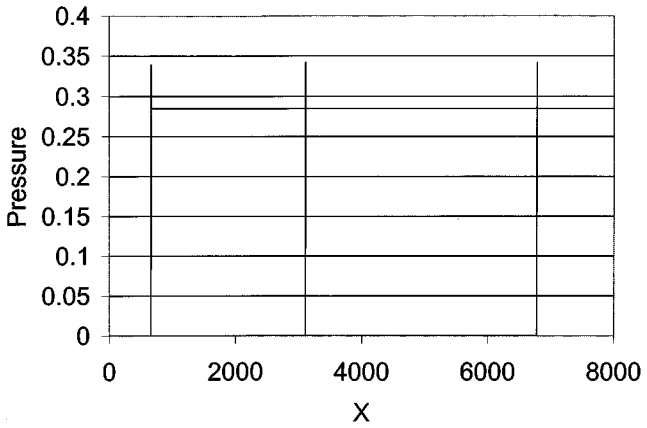

Figure 8. Pressure profiles at t = 1,000; 4,000; and 6,000.

reactant drops from .46 to 6.6×10^{-6} in only six position units, that is a reaction front thickness of 120 μm. Another important aspect is the length of the sample. The detonation only develops after a certain time has elapsed. A condition for detonation is that the time for transition from a deflagration to a detonation should not exceed the time for the compression wave to reach $x = 0$ (where a rarefaction wave will start to unload the system).

If the leading shock reaches the free end $x = 0$, a rarefation wave will start to relax the system and detonation will not be observed.

When $\alpha = 1$, the system detonates and no detonation occurs when $\alpha = 0$. Instead, a simple deflagration is observed, typical for SHS systems. No detonation is found for $E_o = 100$ kJ/mol and $\alpha = 0$ and 1. The higher activation energy excludes detonation behavior, whether the system is sensitive ($\alpha = 1$) or not. A higher impact velocity is required to detonate the system when: (a) the activation energy is high; (b) the system is not sensitive.

Example III

The previous example is repeated for a dimensionless impact velocity of 0.2 and an activation energy of 50 kJ/mol. This impact velocity is not sufficient to ignite systems with $E_o = 100$ kJ/mol ($\alpha = 0$ or 1). The other parameters remain as in Table 1.

First we present results for $\alpha = 1$. In Figure 8 the pressure profiles are shown at t = (1,000; 4,000; 6,000). The spike at the front of the wave is not due to numerical effects; a finer spatial resolution of the graphs shows a distinct high-pressure region. The pressure front and the reaction front lie on top of each other. The chemical energy released in the reaction increases the pressure sharply (second term in EOS) and the pressure in turn couples back into the internal energy by compression—this effect is noticeable in the small temperature spike at the front (Figure 9). A synergism exists between the reaction and shock wave. The temperature profiles (Figure 9) and mass fraction profiles (Figure 10) confirm that a detonation wave, with complete conversion in the shock front, is propagating through the system. The velocity of the detonation remains constant in this case, $D = 1.25$. This corresponds to a dimensional velocity of more than 5 km/s which falls into the expected range for an SHS detonation. The temperature profiles, shown in Figure 9, consist of two regions. In front of the reaction the scaled temperature is zero, while behind the reaction front the temperature reaches a

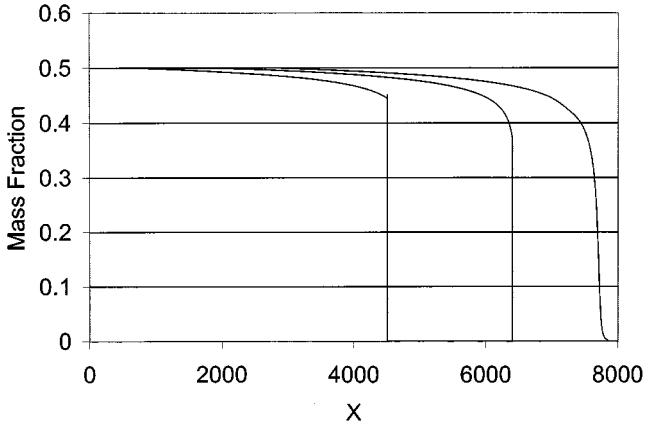

Figure 7b. Mass fraction profiles at t = 4,800; 5,600; and 6,800.

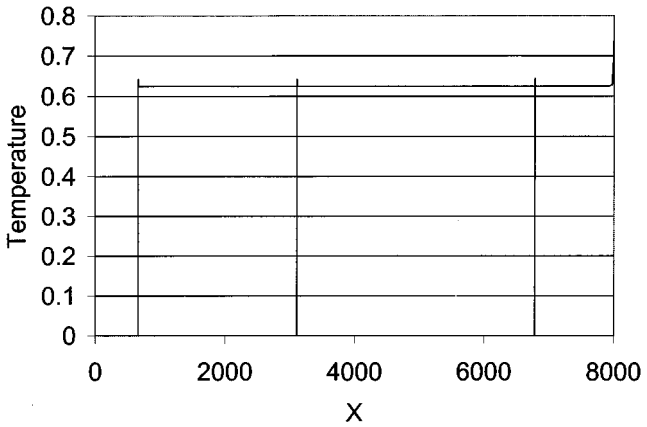

Figure 9. Temperature profiles at t = 1,000; 4,000; and 6,000.

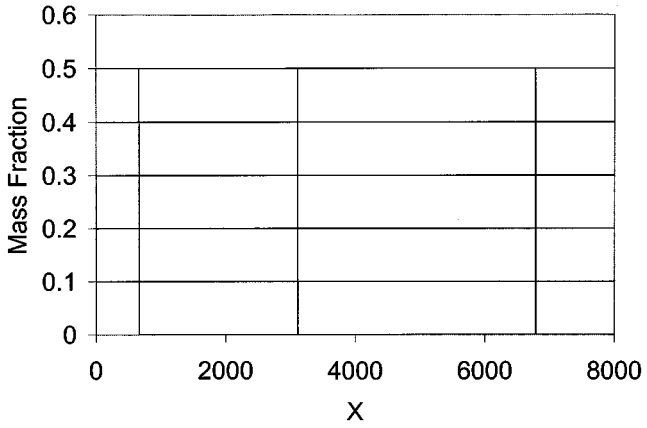

Figure 10. Mass fraction profiles at $t = 1{,}000$; 4,000; and 6,000.

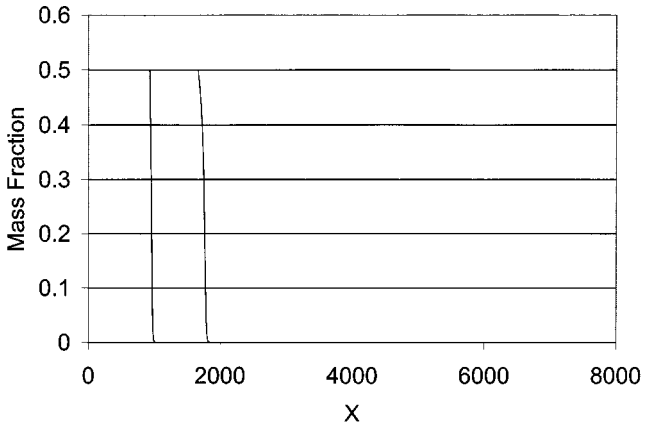

Figure 11b. Mass fraction profiles at $t = 5{,}200$ and 5,800.

steady value of 0.62—this value is less than the (atmospheric pressure) adiabatic temperature rise.

When the numerical experiment is repeated for $\alpha = 0$ (all other parameters remain the same), the impact velocity of 0.2 is not sufficiently high to cause an immediate detonation. Instead, a state that appears closer to Case 2 of Example II is observed. The mass fraction profiles are shown in Figures 11a–11b at $t = (600;\ 1{,}000;\ 4{,}800;\ 5{,}200;\ 5{,}800)$. Complete conversion occurs within the reaction front, but it is difficult to discern the thickness of the front at different points in time.

The pressure profiles are shown in Figures 12a–12c at $t = (600;\ 1{,}000;\ 2{,}000;\ 3{,}200;\ 3{,}400;\ 3{,}600;\ 3{,}800;\ 5{,}000;\ 5{,}200;\ 5{,}400;\ 5{,}600;\ 5{,}800)$. The secondary pressure pulse is already present at $t = 600$, located close to the compression front. At $t = 1{,}000$, the pulse has overrun the compression front and a large pressure spike of $P = 0.77$ is located at the front ($\approx$ 540,000 atm). At $t = 2{,}000$, the pressure peak has receded to $P = 0.4$, dropping more at $t = 3{,}200$. At $t = 3{,}400$, a thickening of the pressure spike is observed. Note the steep gradient on the downstream side and the shoulder forming on the upstream side of the peak. This shoulder develops into another peak that shifts the steep gradient to the upstream side of the peak at $t = 3{,}600$. The peak becomes more focused, and, at $t = 3{,}800$, a single sharp peak exists. The subsequent receding of the peak and upstream shoulder formation are shown at $t = 5{,}000$ through $t = 5{,}400$, followed by another fo-

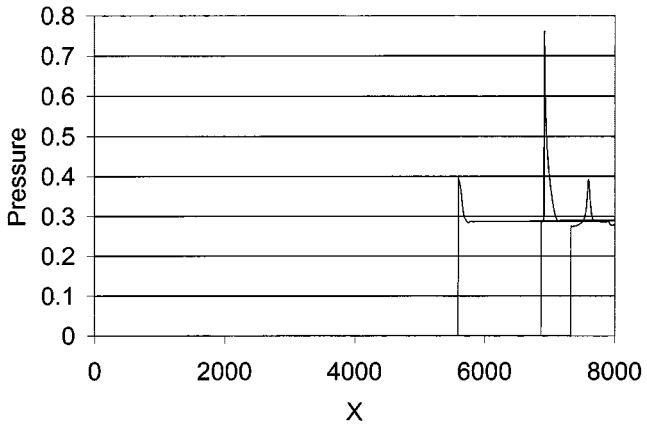

Figure 12a. Pressure profiles at $t = 600$; 1,000; and 2,000.

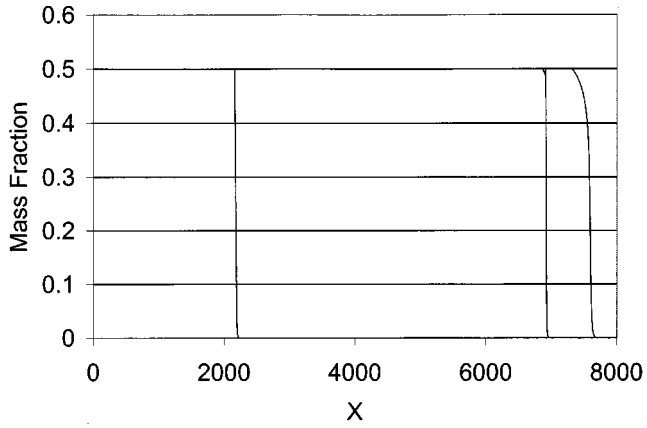

Figure 11a. Mass fraction profiles at $t = 600$; 1,000; and 4,800.

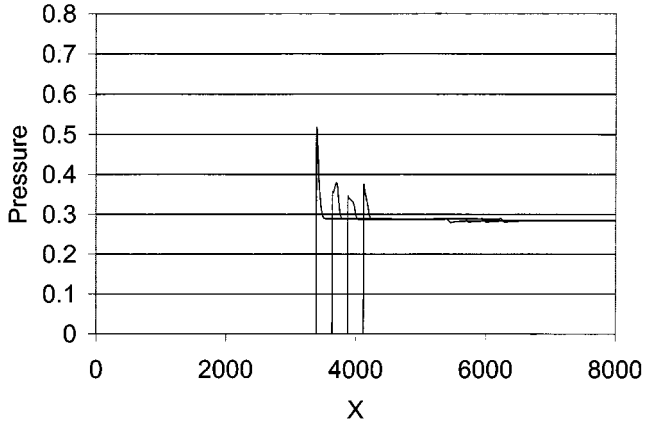

Figure 12b. Pressure profiles at $t = 3{,}200$; 3,400; 3,600; and 3,800.

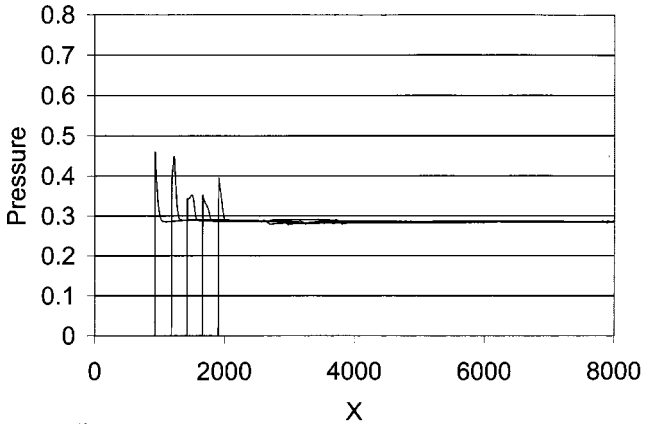

Figure 12c. Pressure profiles at $t = 5{,}000$; 5,200; 5,400; 5,600; and 6,800.

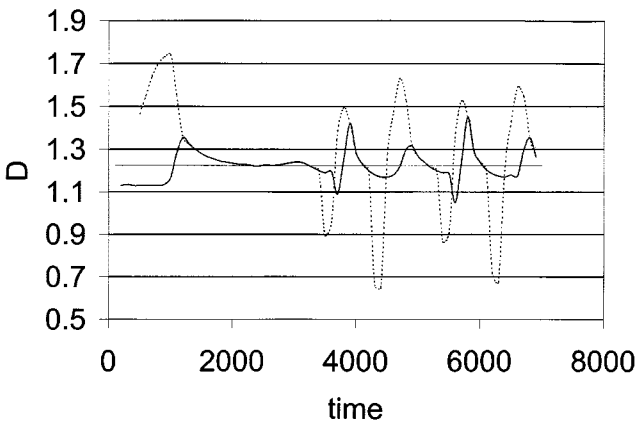

Figure 13. Velocity of compression wave (solid line) and reaction front (dashed line).

cusing through $t = 5{,}800$. The system exhibits oscillatory behavior.

Two important phenomena are present in this example: (1) there is a transition from a deflagration to a detonation in the reaction front; (2) the reaction front and shock front oscillate. Directly after impact, the reaction front travels at subsonic velocity through the system—a typical SHS deflagration. The density at $x = L$ increases after impact (remember there is a jump in the velocity), and, from the first term of the EOS, it follows that a sharp change in pressure occurs, as well. The subsequent temperature rise due to compression is sufficient to ignite the system near the preheated end. The release in chemical energy causes a spike in the pressure. The chain of events is repeated: increased pressure—compression—increased temperature—increased reaction and the pressure pulse propagates through the compressed material (higher sonic velocity) and overruns the initial shock wave. The reaction front reaches velocities of $D = 1.7$ as it approaches the compression wave. Once the reaction front overruns the compression wave, it slows down to an average value of $D = 1.28$, and, simultaneously, the compression front speeds up from $D = 1.12$ to 1.28.

The reaction front does not remain on the compression front at all times. It falls slightly behind, noticeable as a thickening of the pressure pulse at the front and the shoulder formation on the upstream side of the pulse. The reaction front then accelerates toward the compression front again. The position of the reaction front is associated with the pressure pulse that is present behind the compression wave (in some cases the pulse overruns the compression wave and the two fronts overlap). Tracking these positions with time, the velocities of the reaction front and the compression wave can be determined as functions of time. The result is shown in Figure 13. The compression wave velocity is clearly increased by the chemical reaction and it slows down when the reaction front slows down. Note that the maxima and minima velocities of the detonation front lead those of the compression wave. Combined with this fall back and catch up process of the reaction front is associated a thickening and thinning of the reaction front. The behavior is aperiodic, but the time between two consecutive velocity maxima can be estimated as $\approx 1{,}000$ time units (48 μs). Oscillatory detonation is well-known. Shvedov and Dremin (1986) measured these oscillations for black powder and ammonium nitrate-polystyrene mixtures by observing bulges and soot streaks in steel tubes which housed the mixtures.

The calculations for Cases 1 and 2 have also been done without preheating. For these two tests, the initial temperature profiles are set to $T(0, x) = 0$. The change in preheating does not cause an appreciable change in the speed or extent of reaction. The temperature, pressure, and conversion profiles for these tests are nearly identical to those for Cases 1 and 2 of Example III.

Example IV

A higher impact velocity of 0.3 causes detonation in samples with an activation energy of $E_o = 50$ kJ/mol, regardless of consideration of activation energy reduction. Also, the detonation velocity does not change much from earlier samples of detonation, $D = 1.28$, compared to 1.25 in Example II (after detonation has caught up with compression wave). In this example the activation energy is set at 100 kJ/mol and the impact velocity is raised to 0.3; all the other parameters remain the same as before. This activation energy is quite typical for SHS mixtures. When $\alpha = 1$, the system detonates immediately after impact and the behavior is qualitatively the same as Case 1 in Example III. When $\alpha = 0$, the pressure profiles at $t = (3{,}500; 4{,}500; 5{,}000; 6{,}000; 6{,}700)$ are shown in Figures 14a−14b. The transition from a deflagration to a detonation occurs much slower this time (compared to Case 2, Example III). The reaction front increases speed from $D = 1.39$ at $t = 3{,}500$ to $D = 1.62$ at $t = 6{,}700$. The temperature profiles, associated with the same moments in time, clearly demonstrate the effect of the higher impact and are shown in Figures 15a−15b. Consider the profile at $t = 4{,}500$ in Figure 15a. Three zones are identified: (1) a sharp temperature increase due to compression at the position of the shock wave; (2) a continuing increase in temperature behind the shock wave due to chemical reaction (only partial conversion); (3) complete conversion near $x = L$ due to preheating. A localized thermal explosion occurs at $x = L$ and in the profile at $t = 5{,}000$ and following ones, the progression of a secondary (reaction) wave is shown which overtakes the temperature wave associated with compression. Conversion starts in the mate-

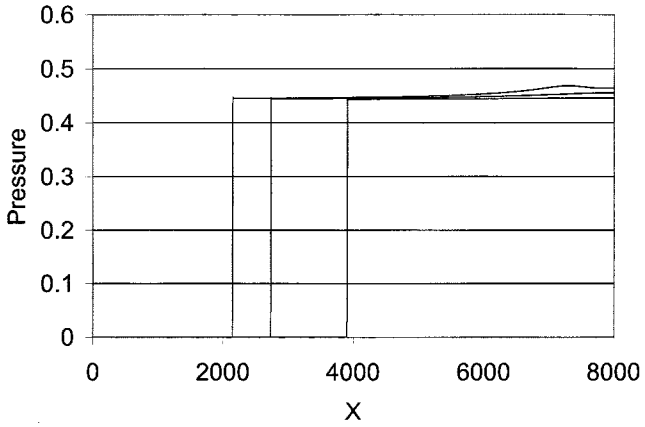

Figure 14a. Pressure profiles at $t = 3{,}500$; 4,500; and 5,000.

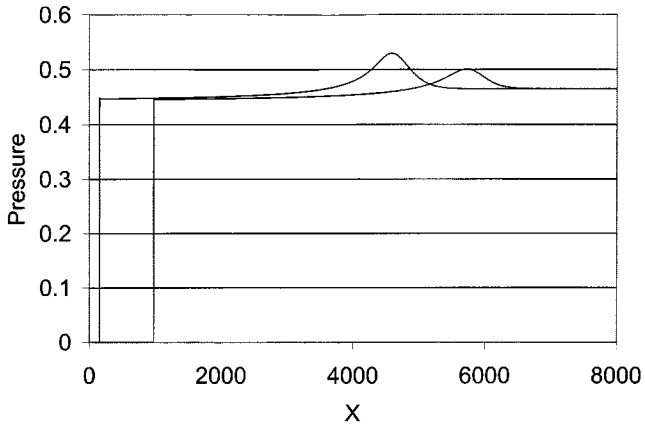

Figure 14b. Pressure profiles at $t = 6{,}000$ and 6,700.

rial with the arrival of the compression wave, and, with the passage of the reaction wave, the conversion is completed.

Example V

In the final example, a system with $E_o = 100$ kJ/mol and $\alpha = 0$ is considered. The impact velocity is 0.4. Pressure profiles at $t = (400; 600; 800; 1{,}800; 3{,}800; 5{,}800)$ are shown in Figures 16a–16b. The reaction front is located directly behind the compression wave, no oscillations are found, and the detonation settles into a constant propagation mode with a velocity of $D = 1.28$. The temperature profiles at the same moments in time are shown in Figures 17a–17b. The slopes

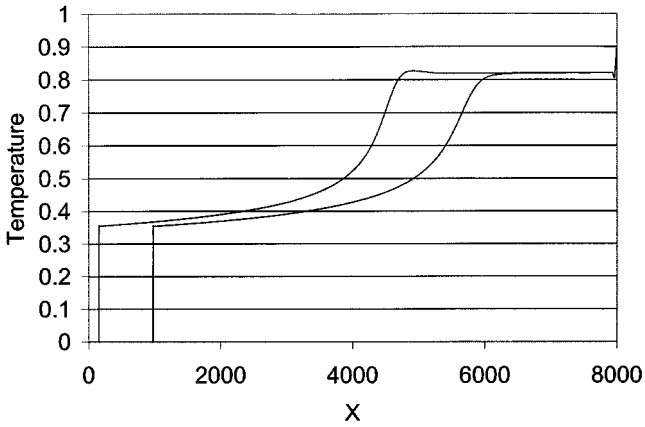

Figure 15a. Temperature profiles at $t = 3{,}500$; 4,500; and 5,000.

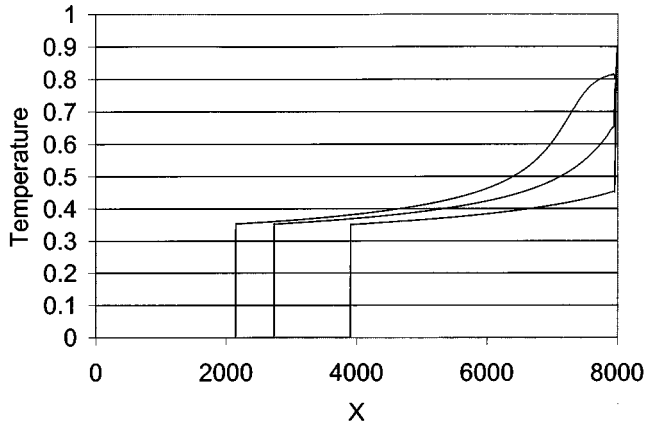

Figure 15b. Temperature profiles at $t = 6{,}000$ and 6,700.

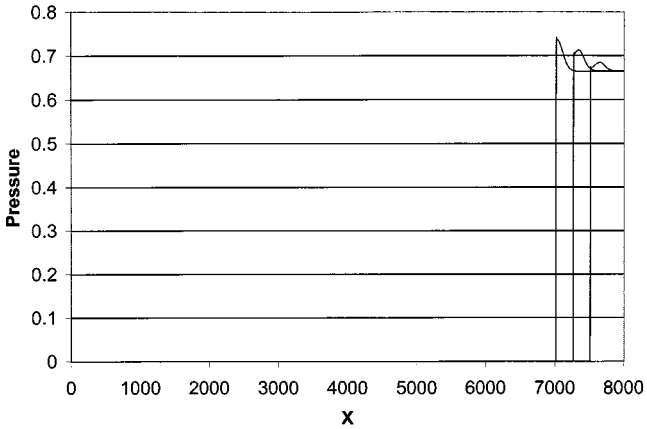

Figure 16a. Pressure profiles at $t = 400$; 600; and 800.

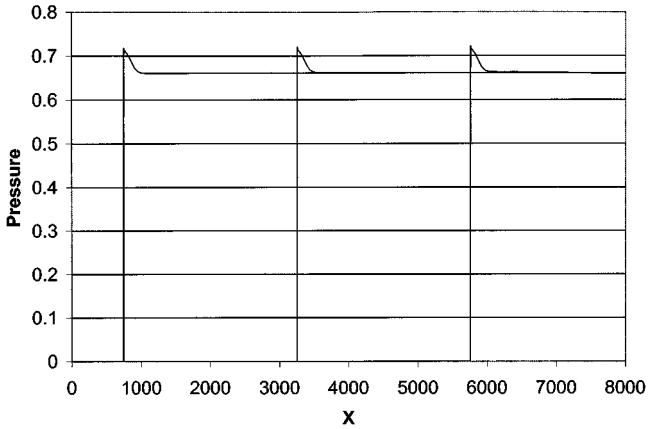

Figure 16b. Pressure profiles at $t = 1{,}800$; 3,800; and 5,800.

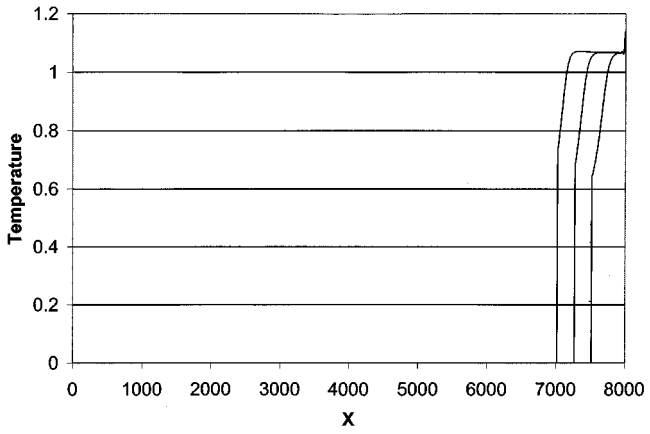

Figure 17a. Temperature profiles at $t = 400$; 600; and 800.

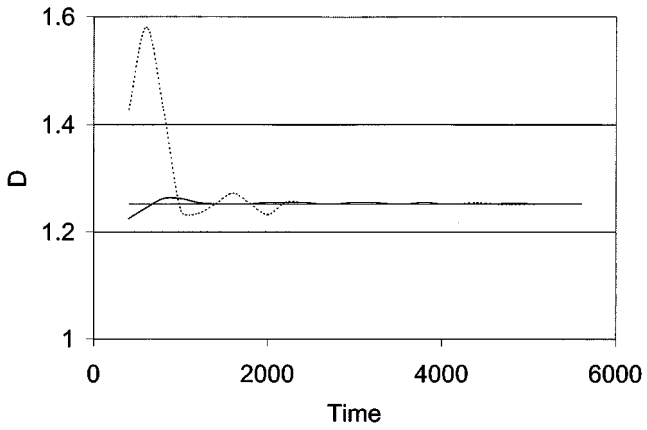

Figure 18. Velocity of compression wave (solid line) and reaction front (dashed line).

of the temperature fronts change between $T = 0.6$ and $T = 0.8$. The first part of the temperature front is associated with heating by compression, followed by reaction until the plateau is reached (complete conversion).

In Figure 18 the velocities of the compression wave and the reaction front are shown. Except for some transient behavior at startup, the two velocities approach a common value $D = 1.28$. This velocity exceeds the compression wave velocity for similar impact of an inert system; hence, the chemical reaction not only sustains the compression wave, but increases its velocity.

Conclusions

A model for reactions in the solid phase has been presented. The stress tensor has been replaced with the state variable pressure, which is valid at conditions above the Hugoniot elastic limit. A two-term equation of state is used to describe contributions of elastic compression and thermal pressure. The kinetics is described by a first-order irreversible reaction. In accordance with the findings of experimentalists, a reduction in the activation energy by elastic compression is also included in the model. This effect is turned on and off by selecting the dimensionless sensitivity parameter $\alpha = 1$ or 0. Two modes of ignition have been investigated: thermal ignition and impact.

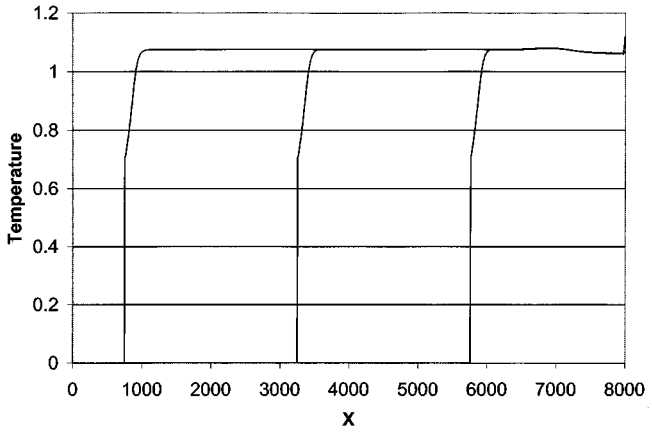

Figure 17b. Temperature profiles at $t = 1{,}800$; 3,800; and 5,800.

In the absence of impact, only a slow deflagration mode of propagation is found. The internal energy and concentration equations become decoupled from the momentum and continuity equations, and the classical SHS models are recovered. The choice of the sensitivity parameter does not affect this result. In other words, a transition from deflagration to detonation by pure thermal pathway has not been found. Elastic compression plays the major role in changing the density and increasing the pressure. In the absence of impact, a weak thermal shock wave propagates through the system (due to instantaneous heating), and the temperature rise associated with this elastic wave is negligible. The significant temperature rise is due to the reaction that propagates slowly.

When the sample impacts a stationary boundary, a shock wave is created. Associated with this shock wave is elastic compression, and an increase in density and a reduction in the particle velocity occur across the front. There is also a significant contribution to the internal energy by compression. The question is whether this increase is sufficient to overcome the activation energy. As expected, the sensitive material detonates at lower impact velocities, and low sensitivity and high activation energy requires stronger impacts. There is a threshold impact below which no ignition occurs. At conditions just above this threshold, ignition is delayed, occurring behind the shock wave. However, the reaction rate accelerates, and a second wave forms which travels faster than the compression wave and overtakes it if the sample is long enough. The reaction front does not approach a fixed positive relative to the compression wave. Instead, an oscillatory state develops where the reaction front falls behind the compression wave then accelerates to catch up with it once more. The period and amplitude (maximum distance between compression and reaction waves) depend on the impact velocity α and E_o (the roles of other parameters have not been investigated). At conditions well beyond the threshold, a steady detonation state is found. The reaction front is located right behind the compression front, and the relative positions remain fixed.

Acknowledgment

HJV wants to acknowledge partial support of this work by the National Science Foundation through grant CTS 9900451.

Notation

C_v = specific heat capacity at constant volume, J/(kg·K)
$Da = (k_o L_s e^{-\gamma})/a_o$
E = activation energy, J/mol
$-\Delta H$ = heat of reaction, J/mol
k = thermal conductivity, W/(m·K)
k_o = pre-exponent rate factor, s^{-1}
R_g = universal gas constant, J/(mol·K)
v = specific volume, kg/m^3
$Z(v)$ = defined by Eq. 11
$\beta_1 = [C_v(T_a - T_o)]/a_o^2$
$\beta_2 = [(-\Delta H) X_{fo}]/a_o^2$
$\beta_3 = [k(T_a - T_o)]/(L_s \rho_o a_o^3)$
$\beta_4 = \alpha_T (T_a - T_o)$
$\gamma = E/(R_g T_a)$
$\sigma = T_o/(T_a - T_o)$

Subscripts

a = adiabatic
c = cold (or isothermal)
o = initial

Literature Cited

Ahrens, T. J., "Equation of State," *High-Pressure Shock Compression of Solids*, J. R. Asay and M. Shahinpoor, eds., Springer-Verlag, New York (1993).

Akhmadeev, N. Kh., "Two-Phase Media Model of Shock Compression with Chemical Reaction," *High-Pressure Shock Compression of Solids IV*, L. Davison, Y. Horie, and M. Shahinpoor, eds., Springer-Verlag, New York (1997).

Aumann, C. E., G. L. Skofronick, and J. A. Martin, "Oxidation Behavior of Aluminum Nanopowders," *J. Vac. Sci. & Tech.*, **B13**, 1178 (1995).

Baer, M. R., "Continuum Mixture Modeling of Reactive Porous Media," *High-Pressure Shock Compression of Solids IV*, L. Davison, Y. Horie, and M. Shahinpoor, eds., Springer-Verlag, New York (1997).

Batsanov, S. S., "Solid Phase Reactions in Shock Waves: Kinetic Studies and Mechanism," *Comb. Expl. & Shock Waves*, **32**, 102 (1996).

Benderskii, V. A., P. G. Filippov, and M. A. Ovchinnikov, "Ratio of Thermal and Deformation Ignition in Low-Temperature Solid-Phase Reactions," *Doklady Akad. Nauk SSR*, **308**, 401 (1989).

Bennett, L. S., Y. Horie, and M. M. Hwang, "Constitutive Model of Shock-Induced Chemical Reactions in Inorganic Powder Mixtures," *J. Appl. Phys.*, **76**, 3394 (1994).

Benson, D. J., V. F. Nesterenko, and F. Jonsdottir, "Numerical Simulations of Dynamic Compaction," *Proc. Net Shape Processing of Powder Materials Symp.*, ASME Int. Mech. Eng. Cong. and Exposition, San Francisco (1995).

Boris, J. P., and D. L. Book, "Solution of Continuity Equations by the Method of Flux-Corrected Transport," *Methods in Computational Physics*, **16**, 85 (1976).

Chen, H. C., J. C. LaSalvia, V. F. Nesterenko, and M. A. Meyers, "Shear Localization and Chemical Reaction in High-Strain, High-Strain-Rate Deformation of Ti-Si Powder Mixtures," *Acta Materialia*, **46**, 3033 (1998).

Danen, W. C., and J. A. Martin, "Energetic Composites," U.S. Patent No. 5,266,132 (1993).

Davis, J. J., A. J. Lindfors, P. J. Miller, S. Finnegan, and D. L. Woody, "Detonation Like Phenomena in Metal-Polymer and Metal/Metal Oxide-Polymer Mixtures," *Eleventh Int. Detonation Symp.*, Snowmass, CO (1998).

Dijken, D. K., and J. Th. De Hosson, "Thermodynamic Model of the Compaction of Powder Materials by Shock Waves," *J. Appl. Phys.*, **75**, 203 (1994).

Enikolopyan, N. S., "Super-Fast Chemical Reactions in Solids," *Russian J. Phys. Chem.*, **63**(9), 1261 (1989).

Enikolopyan, N. S., A. I. Aleksandrov, E. E. Gasparyan, V. I. Skelobkov, and A. A. Mkhitaryan, "Direct Conversion of Chemical Energy into Mechanical without Thermalization," *Doklady Akad. Nauk SSSR*, **319**, 1384 (1991).

Gogulya, M. F., "Interaction of Sulphur and Aluminum Behind Shock Fronts," *Khim. Fiz.*, **11**, 224 (1992).

Graham, R. A., "Comments on Shock-Compression Science in Highly Porous Solids," in *High-Pressure Shock Compression of Solids IV*, L. Davison, Y. Horie, and M. Shahinpoor, eds., Springer-Verlag, New York (1997).

Horie, Y., and M. E. Kipp, "Modeling of Shock-Induced Chemical Reactions in Powder Mixtures," *J. Appl. Phys.*, **63**, 5718 (1988).

Knyazeva, A. G., "Combustion Wave Propagation Through Deformed Solids," *Comb. Explos. and Shock Waves*, **29**, 48 (1993).

Knyazeva, A. G., and E. A. Dyukarev, "Stationary Wave of a Chemical Reaction in a Deformable Medium with Finite Relaxation Time of the Heat Flux," *Comb. Explos. and Shock Waves*, **31**, 37 (1995).

Knyazeva, A. G., "Hot-Spot Thermal Explosion in Deformed Solids," *Comb. Explos. and Shock Waves*, **29**, 3 (1993).

Kovalenko, A. V., and G. V. Ivanov, "Physical and Chemical Transformations of Lead Nitrate in Mixtures with Aluminium under Shock Waves," *Comb. Explos. and Shock Waves*, **17**(4), 141 (1981).

Nesterenko, V. F., M. A. Meyers, H. C. Chen, and J. C. LaSalvia, "The Structure of Controlled Shear Bands in Dynamically Deformed Reactive Mixtures," *Metall. and Mat. Trans. A*, **26**, 2511 (1995).

Nesterenko, V. F., M. A. Meyers, H. C. Chen, and J. C. LaSalvia, "Controlled High Rate Localized Shear in Porous Reactive Media," *Appl. Phys. Lett.*, **65**, 3069 (1994).

Sivashinsky, G. I., "On Spinning Propagation of Combustion Waves," *SIAM J. Appl. Math.*, **40**, 432 (1981).

Shchetinin, V. G., "Calculations of the State Parameters of Condensed Substances at High Pressures and Temperatures," *Comb. Explos. and Shock Waves*, **27**, 39 (1991).

Shlensky, O. F., "Influence of Homogeneous Nucleation on the Rate of Exothermic Thermal Decomposition of Condensed Systems," *Comb. Explos. and Shock Waves*, **31**, 87 (1995).

Shvedov, K. K., and A. N. Dremin, "Explosion Processes Along the Charge in Porous Explosives," *Comb. Explos. and Shock Waves*, **21**, 123 (1986).

Thadhani, N. N., "Shock-Induced Chemical Reactions and Synthesis of Materials," *Prog. in Mat. Sci.*, **37**, 117 (1993).

Thadhani, N. N., A. H. Advani, E. Dunbar, H. A. Grebe, and I. Song, "Shock-Induced Chemical Reactions in *W* and *Re* Powder Mixtures," *High Strain Rate Behavior of Refractory Materials*, R. Ashafani, E. Chen, and A. Crowson, eds., TMS, Warrendale, PA (1991).

Trunin, R. F., *Shock Compression of Condensed Materials*, Cambridge Press, Cambridge (1998).

Varma, A., A. Rogachev, A. Mukasyan, and S. Hwang, "Complex Behavior of Self-Propagating Reaction Waves in Heterogeneous Media," *Proc. Nat. Acad. Sci.*, **95**, 11053 (1998).

Viljoen, H. J., and V. Hlavacek, "Deflagration and Detonation of Solid-Solid Reacting Systems," *AIChE J.*, **43**, 3085 (1997).

Viljoen, H. J., and S. Cohn, "Reaction Driven Elastic Waves in Solid Media," *J. Mat. Syn. and Proc.*, **6**, 107 (1998).

Vreeland, T., Jr., K. L. Montilla, and A. H. Mutz, "Shock Wave Initiation of the Ti_5Si_3 Reaction in Elemental Powders," *J. Appl. Phys.*, **82**, 2840 (1997).

Yano, K., and Y. Horie, "A Numerical Study of Shock-Induced Particle Velocity Dispersion in Solid Mixtures," *J. Appl. Phys.*, **84**, 1292 (1998).

Zel'dovich, Ya. B., and Yu. P. Raizer, *Physics of Shock Waves and High-Temperature Hydrodynamic Phenomena*, Vol. II, Academic Press, New York (1967).

Manuscript received Nov. 9, 1998, and revision received Feb. 12, 1999.